Explosive properties of water in volcanic and hydrothermal systems

Régis Thiery, Lionel Mercury

▶ To cite this version:

HAL Id: insu-00403839

https://hal-insu.archives-ouvertes.fr/insu-00403839

Submitted on 7 Sep 2009

Explosive properties of water in volcanic and hydrothermal systems

R. Thiéry

Laboratoire Magmas et Volcans, UMR 6524, CNRS/Clermont Université,

Clermont-Ferrand, France

L. Mercury

Institut des Sciences de la Terre d'Orléans, UMR 6113, CNRS/Université

d'Orléans, Orléans, France

R. Thiéry, Laboratoire Magmas et Volcans, UMR 6524, CNRS/Clermont Université, 5 rue
Kessler, F-63038 Clermont-Ferrand Cedex, France

L. Mercury, Institut des Sciences de la Terre d'Orléans, UMR 6113, CNRS/Université
d'Orléans, 1A, rue de la Férollerie, F-45071 Orléans Cedex, France

Abstract.   This paper describes, from a thermodynamic point of view, the physico-chemical conditions, under which water behaves as an explosive. This phenomenon occurs frequently in hydrothermal and volcanic systems, when water is brutally shifted from its initial equilibrium state. Water (either liquid or gas) becomes metastable or unstable, and reequilibrates by violent demixing of a liquid-gas mixture. In a first step, a phenomenological approach of metastability is given in an one-component perspective, introducing the notion of spinodals and delimiting the extent of metastable fields. The physical mechanisms (bubble nucleation, cavitation, spinodal decomposition), which are involved in these explosive transformations of water, are detailed in what relates to the natural eruptions topic. The specific thermodynamic properties (P-v-T-H-U) of metastable water are presented by using the reference Wagner and Pruss equation of state. Then, the mechanical work produced by the different possible physical transformations, including decompression, vaporization, isobaric heating and exsolution, involved in water explosions are quantified. The classic calculation of the energy balance under the reversible assumption is here extended proposing a pathway to take irreversibility into account. This model can be used to estimate magnitude of volcanic impacts from scaling laws based on explosion energies.

1. Introduction

Magmatic, volcanic and hydrothermal systems are characterized by an explosive release of energy, which is produced essentially by the mechanical work of expansion of fluids. This explosivity is firstly caused by the exsolution of juvenile, hot and pressurized fluids, mainly composed of water ($> 80\%$ by volume) [*Mills*, 2000], during the magma crystallization and ascent through the crust. This feature is best visualized by the drastic increase of the volumetric fraction (f_v) of exsolved water at near-surface conditions of the Earth (Figure 1), where f_v is computed from the mass fraction of exsolved water (wt % H_2O) by:

$$\text{wt \% } H_2O = \frac{\rho_w \, f_v}{\rho_w \, f_v + \rho_m \, (1 - f_v)}, \tag{1}$$

with ρ_m being the magma density ($\rho_m \simeq 2500$ kg/m^3) and ρ_w, the density of the aqueous phase (in kg/m^3) calculated by the *Wagner and Pruss* [2002] equation of state for water. As pointed out by *Burnham* [1979], more than 3 Gm^3 of steam can be produced from only one Gm^3 of magma exsolving 2 wt % of water at 100 bar. Such a fluid volume cannot be retained on a long period of time under surface, and one of the essential questions of volcanic processes is the evacuation of this excess water out of magmas. The main factor controlling the gas removal is the viscosity of magmas, giving a wide range of contrasted behaviours, from strombolian fountaining to the violent plinian explosions. The most explosive (and sometimes cataclysmic) volcanism arises at the conjunction of both factors, i.e. high water content and high magma viscosity. Figure 1 shows also that the increase of the water volume fraction is accompanied by a marked change of the magma nature, where the silicate melt is fragmented into an aerosol of ash and steam.

Obviously, this transition occurs when the water volume fraction overruns some threshold, which was approximated ca. 50 % by *Wohletz et al.* [1984] or 75-84 % by *Sparks* [1978]. However, recent experimental and theoretical studies [*Thomas et al.*, 1994; *Zhang et al.*, 1997; *Zhang*, 1999; *Spieler et al.*, 2004] have demonstrated the influence of others factors, like the depressurization rates and intensities, the melt viscosities, surface tensions or gas diffusivities on the fragmentation onset. Anyway, this catastrophic exsolution occurs either in the sommital parts of the magmatic chamber just before the eruption, or in the vent during the eruption. The rapid exsolution, decompression and blowing out of these magmatic chambers filled with fluid-rich magmas, leads to the ejection of huge amounts of gas and tephra (pumice and ash), development of pyroclastic falls, flows or surges, and finally, the collapse of a caldera.

The second main cause of explosive eruptions is due to the presence of cold liquid water on the Earth surface. Sudden mixings of large quantities of non-juvenile liquid water with hot materials produce violent explosions, giving rise to a large number of various explosive phenomena (hydroeruptions, [*Moyer and Swanson*, 1987]; surtseyan volcanism, [*Kokelaar*, 1986]; phreato-magmatic eruptions including hydrothermal geysering, [*Browne and Lawless*, 2001]). Additionally, hydrothermal eruptions are not the simple result of liquid water heating, but also require the incidental and sudden decompression of pressurized waters, which are close to their boiling conditions.

Thus, water is the main explosive agent on Earth. For this reason, the properties of water have been the subject of numerous studies, both experimental and theoretical [*Wohletz*, 1983, 1986, 2002; *Zimanowski et al.*, 1991, 1995, 1997b]. In particular, the explosions of water in contact with magma are usually explained by complicated physico-chemical

mechanisms, usually termed "Molten-Fuel-Coolant Interactions" (MFCI) [*Wohletz*, 1983; *Theofanous*, 1995; *Zimanowski et al.*, 1997a]. Despite the abundant litterature, mainly in the volcanological, physico-chemical or industrial engineering fields, these processes are so complex that they are not well understood yet.

In a first part, we will show how water explosions can be described in a general theoretical framework of fluid metastability [*Debenedetti*, 1996]. The notions of so-called spinodal curves, superheated liquids, supercooled gas and others will be introduced, and we will see how these concepts, originating from fundamental physics of fluids, can be useful to understand these eruptive phenomena. Next, the physical mechanisms involved in explosive water reactions will be detailed in what may be used by the volcanological community. Then, the five main energetical contributions involved in magma–water interactions, which are respectively (1) decompression, (2) vaporization, (3) liquid heating, (4) steam heating and (5) magma exsolution, will be quantified by using the reference equation of state for water of *Wagner and Pruss* [2002]. The part of the magmatic thermal energy, which can be transformed into explosive kinetic energy, will be analysed. This will help us to differentiate the different types of hydrothermal and volcanic environments as a function of their explosion energy, calculated according to the one-component water case. Finally, we will show how our model can be used to estimate the intensity of volcanic explosions with the help of scaling laws.

2. What Makes Water an Explosive ?

An explosion is always the violent response of a system to a physico-chemical perturbation, which has left it in an energetic, metastable or unstable, state. For instance, fast thermodynamic processes (water heated at the contact of a magma, rapid depressurisation

83 of a liquid, high-speed flow of a fluid, ...) produce highly transient metastable states,

84 which return towards equilibrium in a very rapid and explosive way. In other words,

85 metastable states are temporary configurations, which are more or less distant from an

86 equilibrium state. The more important is this distance (i.e. the metastability degree),

87 the more explosive will be the relaxation towards equilibrium. As a consequence, the

88 characterization of metastable states can gives us some indications about the explosive

89 feature of physico-chemical transformations.

90   This paper follows a phenomenological approach, based on classical thermodynamics

91 and equations of state. This introduces the notion of spinodals, which are the theoretical

92 bounds between metastability and instability.

2.1. A Phenomenological Approach of Metastability

The thermodynamic properties of a pure substance is described by an equation of state,

which is usually formulated by means of a mathematical formulation of the Helmholtz

free energy A, as a function of the temperature T and molar volume v for pure fluids:

$$A = A(T, v). \tag{2}$$

93 Any thermodynamic parameter can then be obtained by simple differentiation of the

94 $A(T, v)$ function of adequate order [*Thiéry*, 1996].

95   Variables T and v are independent, but one important consequence of the second law

96 of thermodynamics is that some sets of (T, v) values are not allowed. Indeed, to be at

97 internal equilibrium, a fluid of given (T, v) must obey the following relations [*Debenedetti*,

98 1996]:

$$\left(\frac{\partial T}{\partial S}\right)_P > 0, \tag{3}$$

where S is the entropy; and,

$$\left(-\frac{\partial P}{\partial v}\right)_T > 0. \tag{4}$$

Equation 3 is commonly referred to as the thermal stability criterion, and equation 4 as the mechanical stability criterion. Thus, the (T, v) space of a pure compound is splitted into three main regions (Figure 2):

1. the instability field, where neither the thermal nor the mechanical stability criteria 3 and 4 are satisfied. The incidental formation of a fluid with (T, v) properties in the unstable field will be immediately followed by its explosive demixion into a biphasic liquid-gas mixture by a process of spinodal decomposition ([*Debenedetti*, 2000], see Section 2.2).

2. the metastability field, where the fluid phase obeys the stability criteria, but appears to be less stable than a biphasic association. Demixing of the initial fluid (either by partial vaporization or condensation) will proceed by means of nucleation processes (see Section 2.2). The metastable and unstable regions are separated by the spinodal curves. The first spinodal, noted Sp(L), is the liquid spinodal, and is the limit of a metastable (superheated) liquid; whereas the second spinodal, noted Sp(G), is the gas spinodal, limiting the metastable (supercooled) gas field. Both spinodals meet at the critical point.

3. and the stability field, where the fluid is fully stable. Metastable and stable fields are delimited by the binodal curve.

Metastable fields can also be depicted in a (P, T) diagram (Figure 3). The liquid spinodal starts from the critical point and runs to lower pressures with decreasing tempera-

tures (at least, up to 330 K where the liquid spinodal curve exhibits a pressure minimum,

see [*Imre et al.*, 1998] for further details about the topology of the liquid spinodal curve

of water). It is worth to note that the liquid spinodal curve runs through the region

of negative pressures. As a matter of fact, any condensed material can indeed support

negative pressures. Thus, the liquid spinodal curve indicates the highest (theoretical)

tensile stresses that a liquid can bear out. This property of water (and other liquids) has

been well demonstrated by experimental studies of aqueous fluid inclusions [*Zheng*, 1991;

Zheng et al., 1991; *Shmulovich et al.*, 2009]. Note that the field of negative pressure relates

only to the liquid, as negative pressure for gases is a nonsense (due to pressure-density

proportionality, zero gas pressure corresponds to vacuum).

The representation of thermodymanic properties of a fluid in the metastable region is a

highly demanding task for an equation of state, firstly because of the divergence of some

thermodynamic variables (for instance, the isobaric heat capacity), and secondly because

of the scarcity of experimental data. The equation of state of *Wagner and Pruss* [2002]

has been selected, as it is well acknowledged by the scientific community for the liability of

its extrapolation in the metastable field (see [*Wagner and Pruss*, 2002], where its validity

for superheated liquid water is fully discussed). Note however that the equation of state

of *Wagner and Pruss* [2002] yields meaningless results in the unstable field, and care must

be taken to avoid this domain, in particular, for the calculations of spinodals.

2.2. Nucleation-Growth and Spinodal Decomposition

The distinction between metastable and unstable states is closely linked to the type of

relaxation mechanism towards equilibrium. Metastable systems re-equilibrate themselves

by nucleation and phase growth, whereas unstable ones proceed to equilibrium by spin-

139 odal decomposition [*Debenedetti*, 1996, 2000]. This distinction between nucleation and

140 spinodal decomposition is important, as this will control many parameters, such as the

141 incubation time before relaxation, the final distribution of matter, the kinetic rate of the

142 transformation, the rate of energy release and hence its explosivity.

143 Nucleation and spinodal decomposition are both the results of fluctuations of an or-

144 der parameter (i.e. the fluid density for a pure system) describing the system at the

145 microscopic scale. Modalities of phase separation are totally different between these two

146 mechanisms.

147 Spinodal decomposition does not require any thermal activation energy: it is a spon-

148 taneous process, which occurs as soon as the system enters the unstable domain. In-

149 versely, nucleation is an activated process, which will take more or less time to occur in a

150 metastable system.

151 Nucleation is produced by a localized high-amplitude fluctuation of the density. The

152 growth of a small nucleus entails an energy cost as long as a critical size is not attained.

153 The energy barrier E_b, which has to be overcomed for a critical radius r_c, can be approx-

154 imated by the classical nucleation theory (e.g. [*Debenedetti*, 1996]):

$$E_b = \frac{16\,\pi\,\sigma^3}{3\,(P_{\mathrm{vap}} - P_{\mathrm{liq}})^2}, \tag{5}$$

$$r_c = \frac{2\,\sigma}{|P_{\mathrm{vap}} - P_{\mathrm{liq}}|}, \tag{6}$$

155 where σ is the surface tension between liquid and gas, P_{vap} and P_{liq} are respectively the

156 pressure in the gas and liquid phases. The important control parameter is $|P_{\mathrm{vap}} - P_{\mathrm{liq}}|$,

157 which increases from zero at saturation conditions to large values at spinodal conditions.

158 Thus, nucleation is facilitated, when both E_b and r_c become sufficiently small, giving rise

159   to the process of homogeneous nucleation. Thermodynamic spinodal corresponds to nil

160   E_b. Homogeneous nucleation becomes spontaneous as soon as E_b is of the same magnitude

161   order than thermal fluctuations: this is the kinetic spinodal limit [*Kiselev*, 1999; *Kiselev*

162   *and Ely*, 2001], whose curve follows roughly, but shifted at lower temperatures and higher

163   pressures, the theoretical liquid spinodal curve Sp(L) in a (P, T) diagram [*Shmulovich*

164   *et al.*, 2009]. At any condition between saturation and the kinetic spinodal curve, nucle-

165   ation occurs only at some favourable sites, produced by impurities in the fluid or along

166   solid surfaces, where the energy barrier is considerably lowered. This nucleation process

167   is well known under the name of heterogeneous nucleation (e.g. [*Lasaga*, 1998]).

168   Conversely, spinodal decomposition is produced by low-amplitude density fluctuations

169   between adjacent regions in the fluid: slightly more dense domains evolve towards a

170   liquid-like density, and less dense regions evolve towards a gas-like density [*Debenedetti*,

171   1996, 2000]. Because this process involves also the creation of liquid-gas interfaces (which

172   is expensive in energy), only regions of long wavelengths (i.e. covering large areas for

173   a minimal surface cost) will be favoured by these density evolutions at the expense of

174   smaller domains, which will shrink away.

175   In other words, spinodal decomposition is the separation of regions, whose densities

176   are progressively evolving towards two poles, liquid and gas, until stable conditions are

177   reached, whereas nucleation-growth is the formation of new regions from the nucleation

178   sites, but presenting a net density contrast with their surroundings since the beginning.

179   In the case of spinodal decomposition, phase separation occurs throughout the material,

180   whereas phase splitting for nucleation arises only at some nucleation sites and proceeds

181   by means of a reactive interface (either a boiling front or a condensation surface). This

implies slower transformation rates for nucleation-growth, as the growth of the newly nucleated phases requires longer pathways for heat and/or mass transfer. Therefore, the heat and/or mass diffusion may be critical limiting parameters in the nucleation-growth process. On the contrary, spinodal decomposition of liquids into vapours is particularly explosive, as it is accompanied by a partial vaporization and an important energy release in a very short lapse of time. Table 2 summarizes the main differences between these two fundamental kinetic processes of phase separation, which are nucleation-growth and spinodal decomposition. It is worth to note that both mechanisms are not mutually exclusive: a reequilibration transformation of a high-disequilibrium state can start with spinodal decomposition, and then proceed further by the classical mechanism of nucleation-growth. Because the spinodal decomposition of fluids into liquid-gas mixtures is a very rapid process, it cannot be studied experimentally [*Nonnenmacher*, 1980; *Debenedetti*, 2000], except at conditions, which are very close to the critical point.

Very rapid changes of thermodynamic conditions are needed to initiate explosive physical transformations by spontaneous nucleation or spinodal decomposition: these are treated in the next section.

2.3. The Explosive Physical Transformations of Water

Different physical transformations can lead to explosive phenomena (Figure 3): the explosion intensity can be, indeed, visualized by considering the relative positions between the spinodals and the $P - T$ paths undergone by the fluid.

2.3.1. Rapid Heating of Liquid Water

The fortuitous contact of liquid water with a hot surface (at the microscopic scale) is the first way to trigger an explosive boiling. It mainly relates to (1) explosive water-

204 magma interactions [*Wohletz*, 1986; *Zimanowski et al.*, 1986, 1991, 1995; *Wohletz*, 2002],

205 and to (2) steam explosions caused by water spills onto molten metals or salts [*Reid*,

206 1983]. To a first step, all of these processes can be approximated by isobaric heating

207 transformations, i.e. by a horizontal line in the $P - T$ phase diagram of Figure 3, running

208 from the stable liquid field up to the metastable or unstable regions. Extensive laboratory

209 investigations have demonstrated that the boiling temperature T_b of water is the main

210 parameter controlling its explosivity [*Reid*, 1983]: indeed, most explosive boilings are

211 obtained when T_b is, roughly, either around T_{hn} or T_L [*Reid*, 1983]. T_{hn} refers to the

212 temperature of homogeneous nucleation, or the temperature of superheating limit. A value

213 of 577 K (304°C) is usually accepted for the temperature T_{hn} of water at one bar [*Reid*,

214 1983]. T_L is the Leidenfrost temperature [*Leidenfrost*, 1756], at which a thin and stable

215 vapour layer forms at the interface between the hot body and liquid water. Above T_L,

216 this stable vapour layer film constitutes an insulating zone, which prevents any explosion

217 [*Mills*, 1984]. However, a mechanical shock can force contact between liquid water and the

218 hot body, and trigger a violent thermohydraulic explosion [*Zimanowski et al.*, 1991]. A

219 precise and definite value for T_L cannot be given, as it depends on the physical properties

220 of the hot surface, such as its thermal diffusivity, its surface roughness, its prefragmented

221 state and others. Nevertheless, T_L is below the critical temperature T_c of water, and may

222 be as high as the liquid spinodal temperature T_{sp} at 1 bar, ($T_{sp} = 320.45°C = 593.6$ K).

223 Hence, explosive water boilings occur either by spontaneous homogeneous nucleation or

224 by spinodal decomposition. In this latter case, nucleated boiling does not succeed to keep

225 the pace to evacuate the excess heat: this results to a thermal shock and to the spinodal

226 decomposition of the interfacial liquid water.

2.3.2. Liquid Decompressions

Another important cause of fluid instabilities is the rapid depressurization of a liquid, whose $P - T$ path in Figure 3 is represented by a descending vertical line up to a final pressure P_f. But depending upon the initial liquid temperature T_i, this pressure drop can lead to two contrasted evolutions, which we will define as (1) superspinodal decompression and (2) subspinodal decompression. The first case is a decompression in the subcritical region, where the $P - T$ depressurization path cuts the kinetic liquid spinodal in a temperature range, let's say between 250°C ($\simeq 0.8\,T_{hn}$) and T_c, the critical temperature of water ($T_c = 374$°C). As a consequence, the liquid state goes through the metastable field, and subsequently through the unstable field. Such an evolution, which is very rapid, results finally to an explosive vaporization through spinodal decomposition or spontaneous nucleation, which we call a superspinodal decompression.

The second case is a pressure drop of a liquid up to 1 bar, but at a temperature below 250°C. At the difference of the former case, the $P - T$ decompression path does not crosscut the liquid spinodal curve and will produce either non-explosive or moderately explosive boiling, which we refer to as a subspinodal depressurization. This last situation may be also at the origin of cavitation (see next section).

Thus, spinodals are useful to assess the explosive character of a transformation, a conclusion already inferred by engineers dealing with the failure of containers of pressurized liquids. The most serious damages occur, as a rule of thumb, when the temperature of the liquid reservoir is between $0.9\,T_c$ (i.e. roughly $T_{\rm sp}$) and T_c. Such explosions are called BLEVEs, for Boiling Liquid Expanding Vapour Explosions [*Birk and Cunningham*, 1996; *Casal and Salla*, 2006; *Salla et al.*, 2006; *Abbasi and Abbasi*, 2007]. From this temperature

range, one can estimate that the violence of these explosions may be explained, at least in the very first steps, by the spinodal decomposition of superheated liquids induced by a sudden depressurization.

This distinction between subspinodal and superspinodal decompressions may have profound implications on the functioning of hydrothermal systems, as they are subjects to recurring pressure drops up to their lower external pressure P_{ext}. For continental hydrothermal systems, P_{ext} is the atmospheric pressure, whereas for oceanic systems, P_{ext} is the pressure of the sea bottom (mainly between 100 bar and 500 bar for sea floors between 1000 m and 5000 m). Superspinodal liquid depressurizations may occur in eruptions of continental high-temperature and liquid-dominated hydrothermal fields (whose temperatures typically exceed 250°C). The conditions of the largest known hydrothermal eruptions in New Zealand are not known precisely, but maximal explosion focal depths have been estimated up to 450 meters [*Browne and Lawless*, 2001]. This implies incipient boiling at 260°C and 45 bars, i.e. favourable conditions for a nearly superspinodal depressurization against the atmospheric pressure. Phreato-magmatic eruptions produced by deep maar-diatreme systems may also be linked to superspinodal decompressions. To the contrary, subspinodal decompressions are produced by low-temperature continental hydrothermal fields (initial temperature T_i below 250°C) and oceanic hydrothermal fields (final pressure P_f mostly above the spinodal pressure P_{sp}), producing less explosive phenomena, like geysering and biphasic liquid-gas discharges. The contrasted behaviour between subspinodal and superspinodal systems may explain the large temperature difference between oceanic and continental hydrothermal systems. Oceanic hydrothermal fields typically discharge fluids between 300 and 400°C, whereas the temperatures of fluids in continental geothermal

273 fields are lower, mainly between 100°C and 225°C [*Lee*, 2001]. Both mentioned tempera-

274 ture ranges correspond to subspinodal conditions for oceanic and continental fields. This

275 suggests that no hydrothermal field can operate sustainedly in a superspinodal regime.

2.3.3. Cavitation

277 With boiling, cavitation is the other phenomenon associated to subspinodal liquid de-

278 compression, and is a two-step process. In a first step, fast liquid decompressions or

279 high-speed liquid flows create transient and local density perturbations. The liquid pres-

280 sure drops below the saturation pressure or even to negative values. As a result, the liquid

281 is stretched up to a certain point until mechanical failure and apparition of microscopic

282 cavities in the liquid [*Xiao and Heyes*, 2002]. Then, in a second step, the stretched liquid

283 relaxes to equilibrium by elastic rebound. Thus, in the $P - T$ diagram of Figure 3, cavi-

284 tation is represented by two vertical arrows: the first one, downward, indicates the liquid

285 decompression up to the liquid metastable field, and the second one, upward, represents

286 the compressive reaction towards the binodal curve. The vapour inside the cavities fol-

287 lows a similar pressure evolution, i.e. a pressure drop followed by a compression, but with

288 some distinctive features. Firstly, the gas pressure remains always positive. Secondly,

289 the compression leads the gas through the metastable field of supercooled gases, and then

290 through the high-pressure unstable domain of steam. As a consequence, gas bubbles finish

291 up to implode.

292 The implosion of these gas cavities is not without important consequences. The elastic

293 rebound of the surrounding liquid produces a large amount of mechanical energy, which

294 is focused on these microscopic imploding cavities. This process is similar to a stretched

295 string, which hits the hanging wall and transfers to it a significant energy quantity. This

enormous concentration of energy is responsible of a localized and very fast increase of temperatures and pressures (up to 5000 K and 1000 bar [*Suslick et al.*, 1999]), followed immediately by a very rapid cooling. This is the development field of sonoluminescence [*Frenzel and Schultes*, 1934] and sonochemistry [*Caupin and Herbert*, 2006]. Additionally, cavitation allows to explain the formation of some natural geological, but exotic materials, like C_{60} and C_{70} fullerenes [*Phipps Morgan et al.*, 2004] or nanodiamonds [*Ozima and Tatsumoto*, 1997].

The close environment around collapsing cavities exerts also a strong influence on their dynamics. While the implosion of isolated bubbles can be approximated by a spherically symmetrical collapse [*Rayleigh*, 1917; *Benjamin and Ellis*, 1966; *Ohl et al.*, 1999], the dynamics of bubble implosions change drastically at the proximity or contact of a solid surface: the bubble surface is deformed by an involution, which gives rise to an energetic and high-speed liquid jet hitting the solid surface [*Ohl et al.*, 1999]. This phenomenon is similar to Taylor fluid instabilities caused by the collapse of steam films between boiling liquid and a hot surface, which are known to play an important role in water-magma interactions [*Wohletz*, 1986]: as a result, the magma is distorted up to the point to be torn out and fragmented into small bulbous, mossy and nearly spherical clasts, which are typically found in fluidal peperites [*Busby-Spera and White*, 1987].

Cavitation takes too an important part in superspinodal liquid decompressions. *Yu and Venart* [1996]; *Venart et al.* [2004]; *Abbasi and Abbasi* [2007] have demonstrated the existence of another type of explosive liquid decompressions, which have been called BLCBE (Boiling Liquid Compressed Bubble Explosion). These explosions are produced by the failure of a tank containing a pressurized liquid at near-critical conditions, but BLCBE

319 differs from BLEVE by the fact the container does not break off at once. Instead, in a

320 first step, the container failure is limited to the development of a crack through which

321 the depressurizing liquid escapes out. As a result, the initial depressurization wave in

322 the vessel is followed by a reflected compression wave caused by the rapid expansion of

323 the in-situ gas. The subsequent repressurization leads to coherent bubble collapse and

324 cavitation. The implosion of the bubbles generates a shock wave, emitting a high dynamic

325 pressure peak resulting to the final failure of the container. In this sense, BLCBE is a

326 phenomenon relevant for describing the explosive liquid decompressions from hydrother-

327 mal reservoirs and magmatic chambers. In the same category of events, the rarefaction

328 wave following a meteoritic impact [*Ozima and Tatsumoto*, 1997] or a deep-lithospheric

329 eruption (the so-called "Verneshots" of *Phipps Morgan et al.* [2004]) are analoguous cav-

330 itation situations, where a depressurization is followed by a compressive requilibration.

331 As a consequence, cavitation can be considered as one of the fundamental processes of

332 volcanic and hydrothermal systems.

2.4. Expansion of a Gas Under Pressure

333 The sudden decompression of a pressurized gas is undoubtedly an explosive phe-

334 nomenon, whose violence is sufficient to generate shock waves. However, at first sight,

335 this explosion type does not seem to fit our theoretical framework proposed here, where

336 explosions result from spinodal processes. Nevertheless, one can note that the equation

337 of state of the perfect gas ($Pv = RT$) predicts that the $(\partial P/\partial v)_T$ quantity tends to

338 zero for high expansion degrees, indicating a begin of violation of the mechanical stability

339 criterion (see equation 4). Moreover, the surface ($P = 0$) corresponds to a thermody-

340 namic frontier in the $P - v - T$ space of the ideal gas, separating the forbidden domain of

negative pressures from the stable/metastable field of positive pressures. Thus, the limit

($P = 0$) of infinite expansion shares some similarity with the liquid spinodal boundary,

as it generates also a violent explosion.

3. The Explosive Energy of Water

The mechanical energy released by any substance is function of its expansivity through

the classical relation, valid under reversible conditions:

$$\mathrm{d}W = -P\,\mathrm{d}v, \tag{7}$$

where $\mathrm{d}W$ is the amount of mechanical energy produced by the expansion $\mathrm{d}v$ of a

fluid. As a result, the main sources of explosive energy are: (1) the fluid exsolution from

magma by magmatic vesiculation and/or fragmentation (*Burnham* [1979], (2) and the

fluid expansion. Therefore, to quantify the energy balance of volcanism, it is necessary to

differentiate precisely the explosive potential of the five energetic processes of water, which

are respectively (1) liquid expansion by heating, (2) vaporization, (3) steam expansion by

heating, (4) steam adiabatic decompression and (5) water exsolution from magma. We

will see later that these contributions are, indeed, not involved in the same way for the

different types of hydrothermal and magmatic systems. Thus, a close analysis of these

different energetic sources is necessary. We have seen also that water metastability plays an

important role in the explosive character of hydrothermal and volcanic eruptions. Hence,

a last question to be addressed is how metastability modifies the energetic properties of

water.

3.1. The Decompression Energy

Decompression up to the atmospheric pressure is the main source of mechanical energy produced by pressurized fluids. The eruption energy of hydrothermal systems (geysers) or volcanic systems comes principally from the opening and decompression of a deep fluid reservoir, which is suddenly connected to the atmosphere. It may even be proposed that this type of energy is produced during contact of lava with water under atmospheric pressure, as strong transient overpressures can be generated too by boiling of superheated waters [*Zimanowski et al.*, 1995].

The decompression process is so rapid that the system has not enough time to exchange heat with the exterior. Thus, to a first approximation, the decompression is considered to be adiabatic. A further simplification is to state that the decompression is reversible. This is clearly not exact (see below), but this allows to treat the decompression as an isentropic process (i.e., the entropy of the system is constant : $\mathrm{d}S = 0$).

3.1.1. Reversible Conditions

Using the Wagner and Pruss (2002) equation of state, the classic $T - U$ and $T - H$ diagrams (Figures 4 and 5) can be calculated to get a first estimation of the mechanical energy. They include isobaric and isentropic paths extrapolated up to the metastable fields. It can be noted that the isobars exhibit almost linear steep variations in $T - U$ and $T - H$ diagrams, except in the critical and metastable fields, where they depart from their general trends and tend to get horizontal. This behaviour can be explained by the specific properties of fluids in the spinodal and critical fields. Indeed, the slope of an isobar in a $T - U$ diagram is inversely proportional to the isochoric heat capacity:

$$\left(\frac{\partial T}{\partial U}\right)_P = \frac{1}{c_v} \tag{8}$$

In the same way, the slope of an isobar in a $T - H$ is inversely proportional to the isobaric heat capacity:

$$\left(\frac{\partial T}{\partial H}\right)_P = \frac{1}{c_P}. \tag{9}$$

Therefore, the horizontal slopes of isobars in $T - U$ and $T - H$ diagrams are caused by the divergence of isochoric and isobaric heat capacities at spinodal and critical points (e.g. [*Johnson and Norton*, 1991]). The reversible work released by an isentropic fluid expansion can be calculated from the first law of thermodynamics as a function of the internal energy:

$$\mathrm{d}U = T\mathrm{d}S - P\mathrm{d}V = -P\mathrm{d}V = \delta W_{\mathrm{rev}}. \tag{10}$$

The δW_{rev} quantity is conventionally counted as negative, as the system does a work on its surroundings, and so the mechanical work (W_U) is:

$$W_U = \Delta U = U_5 - U_3 < 0, \tag{11}$$

where (3) is the starting state of the decompression and (5) is the final state at atmospheric pressure. Equation 11 is valid for short-lived outbursts. For long-lasting eruptions or fluid flows, the enthalpy is more adapted to the calculation of the mechanical work (for example, the work yielded by a fluid flow in a vent above a magmatic chamber). As a result, the net mechanical work (W_H) of the venting fluid is:

$$
\begin{aligned}
W_H \;=\; & W_U + P_5\,v_5 - P_3\,v_3, \\[4pt]
=\; & H_5 - H_3, \\[4pt]
=\; & \Delta H \le 0. \tag{12}
\end{aligned}
$$

394   where v stands here for the specific volume at the subscribed point.

395   The quantity W_H gives the amount of energy, which can be converted to gravitational

396   potential energy (E_{p}), kinetic energy (E_{c}) and all other forms of mechanical energy (frag-

397   mentation, elastic deformation, shock waves, ...), noted E_{d}. Thus, the energetics of fluid

398   flows and eruption phenomena can be assessed by using a modified form of Bernoulli's

399   equation (Mastin, 1995):

$$
-W_H = \Delta E_{\mathrm{p}} + \Delta E_{\mathrm{c}} + \Delta E_{\mathrm{d}} + {}'\text{frictional terms}'. \tag{13}
$$

400   The last term of this equation takes into account frictions between fluid and the sur-

401   roundings. Depending upon the importance of this frictional term, two contrasted cases

402   can be considered: isenthalpic expansions and isentropic decompressions.

403   **3.1.2. Isenthalpic Decompressions**

404   The so-called isenthalpic fluid expansions are decompressions where all potential and

405   kinetic energies are dissipated through frictions ($W_H = 0$). This situation occurs, in

406   particular, for fluid flows in porous and tortuous media, such as aquifers. The evolution

407   of these flows can be followed on a $T - H$ diagram (Figure 5) along a vertical line starting

408   from the initial point (3). In most cases, isenthalpic decompressions are accompanied by

409   a temperature decrease of the fluid (and a temperature increase of the surroundings). The

410 amplitude of this temperature decrease can be visualized by considering the offset between

411 isobars drawn in Figure 5. Thus, this effect will be particularly marked for supercritical

412 steams (T roughly between 400 and 700°C) and supercooled steams. This property is

413 notably invoked to explain, in part, the heating of the surrounding rocks along pathways

414 followed by steam flows (Armstead, 1978) in geothermal reservoirs.

415 3.1.3. Isentropic Decompressions

416 If the frictional term of equation 13 can be neglected, the expansion can be consid-

417 ered as a reversible isentropic process. To estimate graphically the mechanical work of

418 decompression, isentropic expansion curves must be used. In Figures 4 and 5, several

419 isentropic paths have been plotted. Detailed calculation examples are given for W_U and

420 W_H in Table 3 by using equations 11 and 12. The corresponding paths (Figures 4 and 5)

421 are composed of two parts:

422 1. a first part, at high pressures and temperatures, where the pressure drop runs in the

423 monophasic field, between initial point (3) and point (4). Point (4) marks the demixing of a

424 new fluid phase (liquid or gas). This fluid transition can be located either on the saturation

425 curve (L(G) or G(L) binodal branch), or anywhere along the metastable extrapolation of

426 the isentropic path up to a spinodal point.

427 2. the second part is the decompression in the biphasic liquid-gas domain, up to the

428 atmospheric pressure (point 5).

429 To assess the energetic potential of a pressurized water reservoir, isentropic heat capac-

430 ities $c_{U,S}$ or $c_{H,S}$ can be considered:

$$c_{U,S} = \left(\frac{\partial U}{\partial T}\right)_S, \tag{14}$$

$$c_{H,S} = \left(\frac{\partial H}{\partial T}\right)_S, \tag{15}$$

$_{431}$ ($c_{U,S}$ and $c_{H,S}$ coefficients are inversely proportional to the slope of isentropic paths,

$_{432}$ respectively in $T - U$ and $T - H$ diagrams). Isentropic decompression works W_U and W_S

$_{433}$ can be calculated from these parameters by:

$$W_U = \int_3^5 c_{U,S}\, \mathrm{d}T, \tag{16}$$

$$W_H = \int_3^5 c_{H,S}\, \mathrm{d}T. \tag{17}$$

$_{434}$ As a result, energetic pressurized systems (for a given temperature difference between

$_{435}$ initial and final states) are characterized by elevated isentropic heat capacities. In Fig-

$_{436}$ ures 4 and 5, it can be observed that most energetic isentropic paths are liquid-poor

$_{437}$ steams, featuring the lowest slope in $T - U$ and $T - H$ diagrams ($c_{H,S}$ well above 3 J/K).

$_{438}$ To the opposite, systems, which have a rather low isentropic heat capacity, are super-

$_{439}$ critical steams above 800–900 K ($c_{H,S}$ about 1 J/K) or liquid-rich biphasic liquid-gas

$_{440}$ mixtures ($c_{H,S}$ also around 1 J/K). By performing a study of the energy balance of isen-

$_{441}$ tropic decompressions of gas-liquid mixtures, similar to the one done by *Salla et al.* [2006]

$_{442}$ on isenthalpic expansions, it can be shown that there is a considerable energy transfer

$_{443}$ from the cooling liquid to the expanding steam. Therefore, the high energetic potential

$_{444}$ of wet steams is due to the condensation and cooling of liquid water droplets, providing

$_{445}$ an important energy source (up to 800 J/g of cooling liquid).

446   The relative contributions of monophasic and biphasic decompressions on the expansion

447   work can be also analyzed in separate diagrams. Figure 6 displays the amplitude of the

448   monophasic part $W_{U,1}$ of the mechanical work W_U in a $P - T$ diagram ($W_{U,1} = U_4 - U_3$).

449   The monophasic decompression is especially important for hot and pressurized steams

450   with $W_{U,1}$ values ranging from 200 to more than 1500 J/g. To the contrary, fluids of liquid-

451   like densities have $W_{U,1}$ values below 100 J/g. The influence of the initial pressure on $W_{U,1}$

452   is negligible for a liquid. The intensity of the decompression work $W_{U,2}$ ($W_{U,2} = U_5 - U_4$)

453   of a gas-liquid mixture is displayed in Figure 7 as a function of the saturation temperature.

454   As stated above, this diagram confirms the high energetic potential of saturated steams.

455   Maximum values of $W_{U,2}$ of 655 J/g are obtained for a steam starting to condense around

456   612 K (339°C). Coincidentally, this temperature is quite close to the superheat limit

457   temperature (T_{sp} =593.6 K= 320.45°C) of water.

458   To take an example, steam, initially at a temperature of 1250 K (977°C) and a pressure

459   of 1500 bar (in a reservoir at depth of 6 km), releases an energy W_U of 1000 J/g by decom-

460   pression in the monophasic field (Figure 6). This energy amount is directly consumed to

461   eject the fluid out of the erupting vent. From Figure 6, one reads that its saturation tem-

462   perature is about 500 K (227°C). Therefore, the condensation will probably continue in

463   the atmosphere, where the decompression in the biphasic domain will bring an additional

464   energy quantity about 500 J/g. This energy source should play an important role in the

465   dynamics of pyroclastic surges and flows. In conclusion, the steam expansion releases,

466   theoretically, a total of 1500 J/g, a value which is to be compared with the explosive

467   energy of gunpowder ($\simeq$ 2000 J/g) and TNT ($\simeq$ 4600 J/g). Thus, exsolved steam from a

468   magmatic chamber can be doubtless classified as an explosive substance.

469   At this step, one question arises whether it is more appropriate to use isenthalpic or

470 isentropic conditions to assess the energetic intensity of an explosive process. In an isen-

471 thalpic process, all mechanical forms (gravitational, kinetic, . . .) of energy are converted

472 to thermal energy, which is the fate of any depressurizing system after a certain amount

473 of time. Thus, the isenthalpic assumption is most adequate to characterize the fluid state

474 after complete relaxation. Conversely, in an isentropic process, the final state is fixed at

475 a virtual instant, where the system is charged with energy, but has not yet consumed it.

476 Thus, the isentropic assumption allows to calculate the amount of mechanical works.

477 **3.1.4. Ejecta**

478   To check the validity of the assessment of decompression works by our theoretical model,

479 one can attempt to compare it with volcanological observations by following an approach

480 developed by *Mastin* [1995]. For 1 kg of water interacting with a mass m_r of pyroclasts,

481 the Bernoulli's equation (equation 13) can be detailed to give the decompression work

482 W_H (in J/kg) as:

$$
\begin{aligned}
-W_H \ = \ & (1 + m_r)\, g\, (z_5 - z_3) \\
& + \frac{1}{2}\, (1 + m_r)\, (V_5^2 - V_3^2) \\
& + \,'\text{frictional terms}',
\end{aligned}
\tag{18}
$$

483   where V_3 and V_5 are the respective fluid velocities (in m/s) at points (3) and (5), g is

484 the gravity constant ($g = 9.81$ m^2/s), and z is the altitude. By taking the point (3) as

485 the reference altitude level (i.e. $z = 0$ for the magmatic chamber or the hydrothermal

reservoir), and by assuming that the fluid velocity V_3 is negligible before expansion, one

obtains the general relation linking W_H to the height z and the fluid velocity V:

$$-W_H \simeq 10 \left(1 + m_r\right) z + 0.5 \left(1 + m_r\right) V^2$$

$$+ \,'\text{frictional terms}'. \tag{19}$$

The last term of this equation, labeled 'frictional terms', includes all types of energy,

which are difficult to characterize, i.e. fragmentation, ductile deformation, seismic energy,

blasts . . . . To allow for this, the equation can be rewritten as:

$$-\zeta \, W_H \simeq 10 \left(1 + m_r\right) z + 0.5 \left(1 + m_r\right) V^2, \tag{20}$$

where ζ is a conversion factor of W_H into kinetic and gravitational energies, varying

between 0 and 1. A value of 0.5 can be reasonably assumed for ζ. Thus, the maximum

ballistic height $z_{\max}$ (in m) can be estimated by:

$$z_{\max} \simeq \frac{0.1}{(1 + m_r)} \, \zeta \, |W_H|,$$

$$\simeq \frac{0.1}{m_r} \, \zeta \, |W_H|, \tag{21}$$

or the maximal ejection speed (in m/s) by:

$$V_{\max} \simeq \sqrt{\frac{2 \, \zeta \, |W_H|}{1 + m_r}},$$

$$\simeq \sqrt{\frac{2 \, \zeta \, |W_H|}{m_r}}, \tag{22}$$

or the mass m_r of pyroclasts (in kg) driven by the flow by:

$$m_r \simeq \frac{2\,\zeta\,|W_H|}{V_{\max}^2} - 1,$$

$$\simeq \frac{2\,\zeta\,|W_H|}{V_{\max}^2}. \tag{23}$$

496　Note that in all these equations 21-23, W_H must be expressed in J/kg of water.

497　Vulcanian eruptions are the best studied natural cases, and thus, allow us to compare

498　observed data and model predictions. These eruptions are caused by the brittle failure of a

499　lava dome overlying a pressurized gas zone, which formed either by exsolution of magmatic

500　volatiles or rapid heating of groundwater [*Morissey and Mastin*, 2000]. Several eruptions

501　(Arenal, Costa Rica, 1968; Ngauruhoe, New Zealand, 1975) have been the subject of

502　measurements of ejection velocities of pyroclasts. The maximum velocities range between

503　200 and 400 m/s. By assuming a magma temperature between 1000 and 1200 K, the

504　decompression work W_H of steam initially at pressures below 300 bar can be estimated

505　from Figure 6 between 1100 and 1400 J/g of water. From equation 23 and with a value

506　of 0.5 for ζ, the mass of pyroclasts driven by one kilogram of water can be calculated

507　between 5.9 and 34 kilograms, i.e. a water weight fraction between 2.9 % and 14.5 % for

508　the magma. The reversible assumption leads to somewhat overestimate the water content,

509　although the lowest value is consistent with usual magmatic water contents.

510　**3.1.5. Irreversible Conditions**

511　Irreversibility can be taken into account by using the following general formula [*Planas-*

512　*Cuchi et al.*, 2004], which calculates the final state at point (5) by decompression from

513　point (3):

$$U_5 - U_3 \ = \ -P_{\text{ext}} \left(v_5 - v_3\right),$$

$$= \ -P_5 \left(v_5 - v_3\right), \tag{24}$$

where $P_{\text{ext}} = 1$ bar, and U is the molar internal energy. This equation is consistent with the following formulation of *Zhang* [2000] to allow for irreversibility in volcanic eruptions:

$$H_5 - H_3 = v_3 \left(P_5 - P_3\right). \tag{25}$$

To solve equation 24, two distinct cases must be considered:

1. in the first case, the decompression leads to a stable monophasic system at point (5). The unknown is the value of the temperature T_5 with the constraint that the final temperature T_5 is above the normal boiling temperature ($T_5 > 373$ K). Thus, the process produces superheated steams (note here that the term "superheated" refers to a stable, and not metastable, state of a steam at temperatures above its saturation point, as it is the usage in the geothermics litterature). Therefore we have to numerically solve the equation:

$$U_5(T_5, v_5) - U_3 = -P_{\text{ext}} \left(v_5 - v_3\right). \tag{26}$$

where v_5 is the fluid molar volume at T_5 and 1 bar.

2. in the second case, the decompression leads to a stable biphasic liquid-gas association at $P_{\text{ext}} = 1$ bar and $T_5 = 373.15$ K. Equation 24 becomes:

$$f \, U_{\text{liq}} + (1 - f) \, U_{\text{vap}} - U_3 =$$

$$-P_{\text{ext}} \left[f \, v_{\text{liq}} + (1 - f) \, v_{\text{vap}} - v_3 \right], \tag{27}$$

where U_{liq} (J/mol), v_{liq} (m^3/mol), U_{vap} (J/mol) and v_{vap} (m^3/mol) are all calculated at 373.15 K and 1 bar. The unknown is the value f of the mass liquid fraction in the system and is simply calculated by:

$$f = \frac{P_{\text{ext}} \left(v_3 - v_{\text{vap}} \right) - U_{\text{vap}} + U_3}{U_{\text{liq}} - U_{\text{vap}} + P_{\text{ext}} \left(v_{\text{liq}} - v_{\text{vap}} \right)}. \tag{28}$$

Results are given in Figure 8, which can be compared with Figure 6, where isocurves of the decompression energy and the mass liquid fraction at the final state have been plotted as a function of the initial pressure P_3 and temperature T_3. At initial atmospheric pressures (i.e. $P_3 = P_{\text{ext}}$), the decompression work is zero, whatever the steam temperature. For example, fumarolles have no explosive potential and cannot be exploited economically, except for heat. However, with increasing initial pressure P_3, the mechanical work, which can be extracted by expansion, increases drastically. As shown by the curvatures of the iso-W_U lines, there is an optimal pressure (from 31 bar at 700 K to 81 bar at 1200 K), at which the hot steam can release a maximum mechanical work for a given initial temperature T_3. At pressures higher than 300 bars, the fluid decompression becomes less energetic with increasing pressures, and the temperature becomes the key parameter controlling the mechanical energy content of the fluid.

It can be also observed (Figure 8) that the expansion under irreversible conditions produce final states, which are much more drier, as the result of the internal production of entropy by irreversibility.

545   But most importantly, it can be seen that the assumption of irreversible conditions leads

546 to much smaller values for the decompression energy. Values range from 50 to 550 J/g

547 of water, and represent around one fourth to one third of corresponding energies under

548 reversible conditions. Up to now, reversibility has been almost always applied in the vol-

549 canological litterature [*Wohletz*, 1986; *Mastin*, 1995], with the notable exception of *Zhang*

550 [2000], but irreversibility yields probably more realistic values of the explosive energy, even

551 if it may be somewhat less practical to use. Indeed, the $T-U$ and $T-H$ diagrams cannot

552 be used directly for the irreversible case, except if one uses the approximation of an isen-

553 thalpic process. In Figure 9, the mass liquid fraction of liquid-gas mixtures obtained by

554 decompression up to 100°C and 1 bar of saturated liquid or steam is plotted as a function

555 of the initial temperature for the three possible assumptions, i.e. isentropic, isenthalpic

556 and irreversible cases. As expected, isenthalpic and irreversible depressurizations yield the

557 most dry mixtures, and the isentropic expansion gives the highest liquid fraction. But,

558 interestingly, it can be noted that the isenthalpic hypothesis provides a good approxima-

559 tion of the irreversible case, in particular for the liquid expansion. Thus, it is possible to

560 rely on the isenthalpic decompression model to estimate the mass liquid fraction f of the

561 final state at 100°C and 1 bar, by using the lever rule in the $T-H$ diagram of Figure 5.

562 Then, the irreversible work (in J/g) of decompression of saturated liquid can be given by:

$$
\begin{aligned}
W_U & \simeq P_{\text{ext}} \left[(1-f)v_{\text{vap}} + f v_{\text{liq}} - v_3 \right], \\
& \simeq P_{\text{ext}} (1-f)v_{\text{vap}}, \\
& \simeq 167 (1-f).
\end{aligned}
\tag{29}
$$

563 This expression is accurate with a relative error, which is less than 1 % below 550 K,

564 and the maximum discrepancy does not exceed 4 % at the critical point.

3.2. The Vaporization Work

565 When cold water interacts with hot magma, the first event producing important me-

566 chanical work is vaporization. For one gram of boiling liquid water, the resulting energy

567 is given by:

$$W_{\mathrm{vap}} = -P\left(v_{\mathrm{vap}} - v_{\mathrm{liq}}\right)/M_{\mathrm{H_2O}}, \tag{30}$$

568 where v_{vap} and v_{liq} are the molar volumes of saturated liquid and gas, and $M_{\mathrm{H_2O}}$ is the

569 molar weight of water.

570 The amplitude of this energy is given in Figure 10 as a function of the boiling tempera-

571 ture. Its mean value is around 150 J/g, and it reaches a maximum at 495 K (222°C) and

572 24 bar, where almost 200 J/g can be yielded. This state corresponds to the point of max-

573 imum enthalpy of saturated steam. It is worth to observe that this maximum is obtained

574 at temperatures intermediate between normal boiling temperature and spinodal temper-

575 ature. Thus, the sudden boiling of superheated water at this temperature can give 20 %

576 more mechanical energy than normal boiling at 100°C. To the contrary, when approach-

577 ing near critical conditions, vaporization energy decreases considerably up to zero at the

578 critical point. It is also symptomatic to note that vapour-dominated geothermal systems,

579 such as Larderello (Italia) or The Geysers (California), have pressure-temperature condi-

580 tions which are close to the state of maximum enthalpy for saturated steams [*Goff and*

581 *Janik*, 2000].

3.3. The Heating Work

Fluids expand when they are heated. As such, they exert a mechanical work on their surroundings. Thus, water expansion by heating must be taken into account to assess the energetic balance of water explosions. The case of isobaric heating under reversible conditions will be considered here. In this case, the reversible work can be obtained from a simple difference of the enthalpy and the internal energy:

$$\mathrm{d}H - \mathrm{d}U = P\,\mathrm{d}v = -\delta W. \tag{31}$$

As the pressure is constant and is equal to the pressure of the surroundings ($P = P_{\text{ext}}$), this equation is also valid under irreversible conditions. The variations of the isobaric heating work ($H - U$) is given in Figure 11 as a function of the temperature. Two contrasted behaviours can be observed. First, the heating work of liquids is practically negligible, as demonstrated by the vertical slopes of isobars. The heating of liquid in the metastable field delivers no mechanical work. To the opposite, steams can provide a significant contribution. Isobaric heating curves show a linear trend in the steam field. At low pressures ($P \leq 10$ bar), steam behaves as a perfect gas, and the isobaric expansion work is given by:

$$-W = \Delta(H - U) \simeq R\,\Delta T, \tag{32}$$

where R is the constant of ideal gas for water ($R = 8.31/18 = 0.4617$ J/g/K) and ΔT is the temperature increase. At higher pressures, the slopes of isobars decrease, indicating a higher mechanical energetic potential. For example, at 1000 bar, steam yields almost

twice as more expansion work than under atmospheric pressure for the same temperature increase. Note also that the isobars in Figure 11 include the expansion work produced by vaporization. Thus, as seen in the preceding section, one can recognize in Figure 11 the peak of expansion work released by the vaporization of water at 222°C and 24 bar. Another remarkable property of water is the very high potential of the mechanical expansion work in the critical and the spinodal field of supercooled gases, as illustrated by the nearly horizontal slopes of isobars.

To summarize, contact of cold liquid water with a hot body, like a basaltic flow, can produce a mechanical work up to 600 J/g. As a result, vaporization and steam isobaric heatings represent also significant energetic contributions of a water explosion.

3.4. The Exsolution Work

The exsolution work of water from magmas is another important source of energy, which must be taken into account in magmatic systems. Indeed, the exsolution is accompanied by a net volume increase from the partial molar volume $\overline{v}_{H_2O}$ of water to the molar volume v of steam under the (P, T) exsolution conditions. Experimental data indicate that the partial molar volume $\overline{v}_{H_2O}$ in hydrous silicate glasses is around 12 ± 0.5 cm^3/mol at room temperature [*Richet et al.*, 2000; *Richet and Polian*, 1998]. With a partial molar thermal expansion coefficient of H$_2$O about 4×10^{-5} [*Richet et al.*, 2000], a temperature increase of 1000 K leads only to an augmentation of 4 % of $\overline{v}_{H_2O}$, i.e. 0.5 cm^3/mol. Inversely, a pressure increase leads to a small decrease of $\overline{v}_{H_2O}$. Thus, we have retained a mean value of 12 cm^3/mol for $\overline{v}_{H_2O}$ for the ranges of magmatic temperatures and pressures considered here (900 K $< T <$ 1600 K and 1 bar $< P <$ 3000 bar).

620   To determine the exsolution work, the first idea would be to apply the same rigorous

621 algorithms described in section 3.1.1 for a reversible process or section 3.1.5 for an ir-

622 reversible one. However, no equation of state has been yet developed to describe the

623 energetic properties of hydrous magmas, neither for its internal energy or its enthalpy.

624 Thus, the trade-off is to focus only on the isothermal and isobaric exsolution work W_{ex}

625 under the pressure-temperature conditions (P_3, T_3) in the magmatic chamber or at the

626 fragmentation level in the volcanic conduit:

$$W_{\text{ex}} = -P_3 \left(v_{\text{vap}} - \overline{v}_{\text{H}_2\text{O}} \right), \tag{33}$$

627   where v_{vap} is the molar volume of steam calculated by the Wagner and Pruss equation of

628 state [*Wagner and Pruss*, 2002] at (P_3, T_3) conditions. Values of the exsolution work are

629 given in Figure 12. They range between 250 and 700 J/g of exsolved water. This represents

630 a notable energetic contribution of magmatic systems (almost the double of the steam

631 expansion work for a basaltic magma). The exsolution energies show rather a stronger

632 dependence with respect to the temperature than to the pressure, except at pressures

633 below 500 bar. The bulk explosion energy of a magmatic eruption is then estimated

634 by the sum of W_{ex} and the expansion work W_U, calculated either under the reversible

635 assumption (section 3.1.1, equation 11) or under the irreversible hypothesis (section 3.1.5,

636 equation 24). For instance, a basaltic lava exsolving 1 weight percent of water at the earth

637 surface produces only an exsolution energy of 5.5 J/g of magma at 1200 K (i.e. 550 J/g

638 of water from Figure 12) and no steam expansion work at all (Figure 8). The same

639 magma, exsolving in a magmatic chamber at a pressure of 500 bar generates 500 J/g of

640 exsolved water and 420 J/g of water by irreversible decompression against the atmospheric

pressure, that is 920 J/g of water or 9.2 J/g of magma and per weight percent of exsolved

water. Our model can also be applied to the 18 May 1980 eruption of the Mount St-

Helens by using the parameters of *Zhang* [2000]: $T_3 = 1200$ K (927°C), $P_3 = 2200$ bar

and a weight percent of exsolved water of 3.7 %. By assuming that the melt is entirely

expelled by exsolving water, we estimate the mass of pyroclasts $m_r = (1000-37)/37 = 26$

kg for one kg of steam. From Figure 8, the irreversible decompression work is found to

amount to 320 J/g of exsolved water, whereas from Figure 12, the exsolution work ranges

between 420 J/g of exsolved water (exsolution at (P_3, T_3)) and 550 J/g of exsolved water

(exsolution under the atmospheric pressure). This gives us a total mechanical work W

between 740 and 870 J/g of exsolved water. From equation 22, we calculate a maximal

ejection speed $V_{\max}$ between 165 m/s and 180 m/s by assuming an energy conversion

factor ζ of 0.5. These values are in agreement with estimations of 100-110 m/s of the

choked exit velocity [*Kieffer*, 1981] or with measurements of 150 m/s for the velocity of

the lateral explosion cloud [*Friedman et al.*, 1981; *Voight*, 1981].

3.5. The Explosion Power

Up to now, we have discussed about the water explosivity in terms of energy quantities.

However, what makes a good explosive is not the amount of work involved, but the

production rate of work per time unit, in other words, its power or, equivalently, its yield

expressed in mass of TNT. The explosivity of water is due to a physical transformation,

the rate of which is a function of its metastability degree. The duration of explosive

reactions between water and magma is on the order of the millisecond [*Zimanowski et al.*,

1991, 1995], thus an explosive vaporization of 500-1000 J/g represents a power of 500 kW

to 1 MW/g of water. The magnitude of this phenomenon is 3 to 4 orders higher than usual boiling conditions.

4. A Typology of Hydrothermal and Volcanic Systems

The preceding section have analyzed the different energetic contributions, i.e. fluid expansion accompanied or not by vaporization/condensation processes, isobaric boiling, and magmatic exsolution, and their explosive potentials have been discussed. A synthesis of their relative contributions in hydrothermal and volcanic systems can be done in a pressure-enthalpy diagram (Figure 13). The different cases are produced by the interactions in various proportions of (1) meteoric, superficial and connate waters, whose $P - T$ conditions are close to the mean geothermal gradient (left part), and (2) ascending magmas in the upper part of the crust, either intruding or extruding, (right part). Energy estimations given below are based on values calculated under the irreversibility assumption.

1. First, one can consider liquid-dominated geothermal systems, (A in Figure 13). The boiling must be triggered by a depressurization of the geothermal reservoir [*Armstead*, 1978]. Thus, the energy source comes mainly from the liquid boiling and steam expansion, well below 100 J/g of H_2O (see equation 29 and Figure 7). Moreover, their explosive potential is weak and is mainly represented by geysers (subspinodal decompressions).

2. Next (B in Figure 13), these are supercritical or slightly subcritical fluids, typically found in the lithocaps of magmatic chambers [*Norton and Dutrow*, 2001], or in deep geothermal systems (black smokers of oceanic ridges). Sudden pressure drops on such systems up to atmospheric conditions are expected to lead to superspinodal decompressions and produce explosions of high power (for instance, see the isentropic decompression

curve labeled 700 K, which intersects the liquid spinodal curve in Figure 13). Such events would involve a mechanical energy of 150–200 J/g of H_2O (Figure 8).

3. Then, vapour-dominated geothermal systems (C in Figure 13) produce mechanical energy by expansion of gaseous fluids, below 150 J/g of H_2O (Figure 7). Well-known examples include the geothermal fields of Larderello (Italia) or The Geysers (California). The deep parts and the porous spaces of these geothermal fields contain saturated waters in larger proportions than steam [*Goff and Janik*, 2000]. Steam migrates upwards in the fractures by isenthalpic boiling, but the condensing liquid separates and percolates deeper. As a consequence, steam evolves progressively towards the state of maximum enthalpy.

4. In the field labeled D are found fluids exsolved by magmas during their cooling and crystallization in a magmatic chamber, a few kilometers below the surface. These are volatile-rich magmas, as well as hot and pressurized fluids. The mechanical energy of of vulcanian and plinian volcanisms is produced by magmatic exsolution (450–600 J/g of H_2O) and steam expansion (from 200 J/g to 400 J/g of H_2O, Figure 8).

5. And finally, liquid waters (E) which are suddenly heated by contact with hot magmatic lavas at Earth surface. This includes surtseyan volcanism and superficial phreato-magmatism. The mechanical work is mainly produced by heating, and amounts to levels between 200 and 600 J/g of H_2O (Figure 11). Moreover, explosive boiling of water can create transient overpressures, probably of several ten bars [*Zimanowski et al.*, 1995]. Thus, the irreversible decompression of these fluids will give an additional energy amount between 100-300 J/g (Figure 8).

Note that the bulk energy released by phreato-magmatism can be as high as in plinian volcanism. However, a correct assessment of the energy of a phreato-magmatic explosion

707   requires a global analysis of the energy balance, as carried out by *Wohletz* [1986], that is

708   based on the determination of the interactive water–magma mass ratio.

5. Geophysical Application: Estimation of Volcanic Impacts

In the same way than the thermodynamic models of *Wohletz* [1986, 2002] and *Mastin*
[1995], our model can be applied to case studies of volcanic and hydrothermal erup-
tions. Volcanic impacts can be approximated from a few number of scaling laws, using
the explosion yield, expressed in tons of TNT. For instance, it is possible to estimate
the overpressure of the blast [*Kingery and Pannill*, 1964; *Taniguchi and Suzuki-Kamata*,
1993], the diameter of the crater [*Nordyke*, 1962; *Wohletz and Heiken*, 1992; *Goto et al.*,
2001] or the height of the explosion cloud [*Ohba et al.*, 2002]. These similarity rules are
mostly based on a cubic root formulation:

$$R = R_0 \, W^{1/3}, \tag{34}$$

709   where R is the distance from the explosion center, at which an event of given intensity is

710   observed; R_0 is a scaling parameter and W is the explosion energy. The scaling parameter

711   R_0 is usually derived from correlations established from impact studies of explosions of

712   energy W_0 (either chemical explosives [*Van den Berg and Lannoy*, 1993] or nuclear bombs).

713   In general, these methods must be used with caution [*Browne and Lawless*, 2001], and,

714   in particular, their application must take care of specified validity conditions (explosive

715   type, site geometry, confinement, explosion depth and others . . .).

716   One application example can be made on the study of *Ohba et al.* [2007] about a small

717   phreatic eruption on the flank of a dacite lava dome of Akita Yakeyama, northern Honshu,

718   Japan, which occured in 1997 and lasted for 70 minutes. The source of eruption was a

719 hot aquifer, situated at about 1000 m of depth at a temperature ca. 300–350°C and a

720 pressure between 110 and 240 bar. The explosions were triggered by initial mud effusions

721 from the overlying plumbing system, which released the pressure in the deep reservoir.

722 Therefore, the explosions extract their energy from the boiling and steam expansion.

723 The bulk volume of muddy materials involved in the eruption was estimated around

724 1000 m^3 with an initial water contents of 18–20 wt.%, a rock density of 2400 kg/m^3 and a

725 water density between 580 and 720 kg/m^3. From these parameters, we can estimate the

726 mass of explosive liquid water between 300 and 320 tons. From Figure 7, the explosion

727 energy can be estimated between 242 and 370 J/g of H_2O under the classical reversibility

728 hypothesis, and between 68 and 93 J/g of H_2O by assuming irreversibility. This yields a

729 bulk explosive work between 72 and 120 GJ for a reversible process, which is somewhat

730 below the estimations of *Ohba et al.* [2007] between 100 and 200 GJ by using the method

731 of *Mastin* [1995]. The irreversibility hypothesis gives an estimate between 20 and 28 GJ.

732 *Ohba et al.* [2007] used also similarity rules to estimate the energy of discrete explosions

733 from the size of one of the craters [*Nordyke*, 1962; *Goto et al.*, 2001] and from the height of

734 the observed clouds [*Ohba et al.*, 2002]. The energy of the largest explosions was estimated

735 between 3 and 5 GJ by *Ohba et al.* [2007]. Thus, our estimates of the bulk explosive energy

736 remain consistent with the similarity models used by *Ohba et al.* [2007]. Figure 8 can also

737 be used to evaluate the mass of vapour produced by the eruption. One obtains mass

738 fractions of steam, between 32 and 41 weight % for an isentropic process, and between 41

739 and 54 weight % for an irreversible one. Both estimates are coherent with the muddiness

740 of air-fall deposits. From Figure 13, one can note that the aquifer of the Akita Yakeyama

741 volcano is just near or inside the shaded area of the explosive field of the $H - P$ diagram.

This fact is well confirmed by the explosive nature of this hydrothermal system, which

contrasts markedly from geothermal ones of lower temperatures. As noted by *Ohba et al.*

[2007], the craters are produced by the shallow explosions of the ascending and bubbling

muds at depths of 6-10 m, corresponding to near atmospheric pressures ca 1–2 bar. By

referring to the $P - T$ diagram of Figure 4, it can be noticed that the irreversible and

adiabatic (and nearly isothermal) decompression path of these fluids at initial 300–350°C

runs near the liquid spinodal curve Sp(L) at these surficial levels. Hence, it is suggested

to associate the explosion focus to a "spinodal" zone, where the metastable bubbly muds

reequilibrate violently by intensive spontaneous bubble nucleations and expansions. This

conclusion could be well justified by the muddy nature of these fluids, featuring probably

important concentration gradients and high viscosities, which delay their reequilibration

with respect to external changes. In the classification of *Zhang* [2000], such a system tends

to a "dynamically completely irreversible" behaviour, which is the trademark of explosive

systems.

6. Conclusion

Rapid physical transformations (mainly magma exsolution, steam decompression or

heating) are the causes of strong water instabilities, which lead to the explosive mani-

festations featured by hydrothermal and magmatic systems. These explosive properties

of water have been treated here from a macroscopic point of view by using basic and

fundamental concepts (yet rarely used in the volcanological litterature), such as metasta-

bility and spinodals. This approach can be fruitful to predict the explosive character of a

transformation, here based on an one-component perspective. As a result, this allows us

to differentiate superspinodal transformations, which are highly explosive (e.g. BLEVE),

and subspinodal ones, which are non or moderately explosive (e.g. cavitation or geyser-ing). The adopted phenomenological point of view can be linked to the more common kinetic approach, as the physical mechanism of equilibrium relaxation differ also between metastable systems (nucleation-growth process) and unstable ones (spinodal decomposi-tion).

The specific energetic properties of water have been presented both in the metastable and stable domains with the help of the Wagner and Pruss equation of state [*Wagner and Pruss*, 2002]. The mechanical work of the different possible physical transformations, in-cluding decompression, boiling, isobaric heating and magma exsolution has been assessed both under the reversibility and irreversibility assumptions. Up to now, the reversibility hypothesis has been almost always used for quantifying the energy balance of eruptions. Here is proposed a pathway to do calculations under the irreversible assumption which results in more realistic estimates. Then, a classification of the hydrothermal and vol-canic systems has been proposed by taking into account their energetic balance and their explosivity. Finally, we show how the model can be used in conjunction with empirical scaling laws to predict potential impacts of volcanic eruptions.

786 programs used in this work can be found at the following address: `http://wwwobs.`

787 `univ-bpclermont.fr/lmv/pperm/thiery_r/index.html`.

References

788 Abbasi, T., and S. Abbasi (2007), The boiling liquid expanding vapour explosion

789 (BLEVE): Mechanism, consequence assessment, management, *Journal of Hazardous*

790 *Materials*, *141*, 480–519, doi:10.1016/j.jhazmat.2006.09.056.

791 Armstead, H. (1978), *Geothermal energy, its past, present and future contributions to the*

792 *energy needs of man.*, Spon Ltd, London.

793 Benjamin, T., and A. Ellis (1966), XX. The collapse of cavitation bubbles and the pres-

794 sures thereby produced against solid boundaries, *Phil. Trans. R. Soc. Lond. A*, *260*,

795 221–240.

796 Birk, A., and M. Cunningham (1996), Liquid temperature stratification and its effect on

797 BLEVEs and their hazards, *Journal of Hazardous Material*, *48*, 219.

798 Browne, P., and J. Lawless (2001), Characteristics of hydrothermal eruptions, with ex-

799 amples from New Zealand and elsewhere, *Earth-Science Reviews*, *52*, 299–331.

800 Burnham, C. (1979), Magmas and hydrothermal fluids, in *Geochemistry of hydrothermal*

801 *ore deposits*, edited by H. Barnes, pp. 71–136, Wiley, New York.

802 Busby-Spera, C., and J. White (1987), Variation in peperite textures associated with

803 differing host-sediment properties, *Bull. Volcanol.*, *49*, 765–775.

804 Casal, J., and J. Salla (2006), Using liquid superheating for a quick estimation of over-

805 pressure in BLEVEs and similar explosions, *Journal of Hazardous Materials*, *A137*,

806 1321–1327, doi:10.1016/j/jhazmat.2006.05.001.

807 Caupin, F., and E. Herbert (2006), Cavitation in water: a review, *C. R. Physique*, *7*,

808 1000–1017.

Debenedetti, P. (1996), *Metastable Liquids*, 411 pp., Princeton University Press, Princeton, New Jersey.

Debenedetti, P. (2000), Phase separation by nucleation and by spinodal decomposition: Fundamentals, in *Supercritical Fluids: Fundamentals and Applications*, edited by K. Kiran, P. Debenedetti, and C. Peters, Nato Science Series E, pp. 123–166, Kluwer Academic Publishers, Dordrecht/The Netherlands.

Frenzel, H., and H. Schultes (1934), Luminescenz in ultraschallbeschickten Wasser, *Z. Phys. Chem.*, *27b*, 421–424.

Friedman, J., G. Oehloeft, G. Johnson, and D. Frank (1981), Heat content and thermal energy of the June dacitic dome in relation to total energy yield, May-October 1980, in *The 1980 Eruptions of Mount St. Helens, U.S. Geol. Surv. Prof. Paper*, vol. 1250, edited by P. Lipman and D. Mullineaux, pp. 557–567, Washington, U.S.

Goff, F., and C. Janik (2000), Geothermal systems, in *Encyclopedia of volcanoes*, pp. 817–834, Academic Press.

Goto, A., H. Taniguchi, M. Yoshida, T. Ohba, and H. Oshima (2001), Effects of explosion energy and depth to the formation of blast wave and crater: field explosion experiment for the understanding of volcanic explosions, *Geophys. Res. Lett.*, *28*, 4287–4290.

Imre, A., K. Martinas, and L. Rebelo (1998), Thermodynamics of negative pressures in liquids, *J. Non-Equilib. Thermodyn.*, *23*(4), 351–375.

Johnson, J., and D. Norton (1991), Critical phenomena in hydrothermal systems: state, thermodynamic, electrostatic, and transport properties of H_2O in the critical region, *American Journal of Science*, *291*, 541–648.

831   Kieffer, S. (1981), Fluid dynamics of the May 18, 1980 blast at Mount St Helens, in *The*

832   *1980 Eruptions of Mount St. Helens*, *U.S. Geol. Surv. Prof. Paper*, vol. 1250, edited by

833   P. Lipman and D. Mullineaux, pp. 379–401, Washington, U.S.

834   Kingery, C., and B. Pannill (1964), Peak over-pressure vs scaled distance for TNT surface

835   burst, *Tech. Rep. 1518*, Aberdeen.

836   Kiselev, S. (1999), Kinetic boundary of metastable states in superheated and stretched

837   liquids, *Physica A*, *269*, 252–268.

838   Kiselev, S., and J. Ely (2001), Curvature effect on the physical boundary of metastable

839   states in liquids, *Physica A*, *299*, 357–370.

840   Kokelaar, B. (1986), The mechanism of surtseyan volcanism, *J. Geol. Soc. London*, *140*,

841   933–944.

842   Lasaga, A. (1998), *Kinetic Theory in the Earth Sciences*, Princeton, New Jersey, 811 pp.,

843   Princeton University Press.

844   Lee, K. (2001), Classification of geothermal resources by exergy, *Geothermics*, *30*, 431–442.

845   Leidenfrost, J. (1756), On the fixation of water in diverse fire. Duisburg. In German; trans.

846   Wares C. 1966., *International Journal of Heat and Mass Transfer*, *9*, 1153–1166.

847   Mastin, L. (1995), Thermodynamics of gas and steam-blast eruptions, *Bull. Volcanol.*, *57*,

848   85–98.

849   Mills, A. (1984), Pillow lavas and the Leidenfrost effect, *J. Geol. Soc. London*, *141*, 183–

850   186.

851   Mills, M. (2000), Volcanic aerosol and global atmospheric effects, in *Encyclopedia of vol-*

852   *canoes*, edited by H. Sigurdson, Academic Press.

Morissey, M., and L. Mastin (2000), Vulcanian eruptions, in *Encyclopedia of volcanoes*, pp. 463–475, Academic Press.

Moyer, T., and D. Swanson (1987), Secondary hydroeruptions in pyroclastic-flow deposits: examples from Mount St Helens, *J. Volcanol. Geotherm. Res.*, *32*, 299–319.

Nonnenmacher, T. (1980), On the kinetics of spinodal decomposition, *Z. Physik B – Condensed Matter*, *38*, 327–333.

Nordyke, M. (1962), An analysis of cratering data from desert alluvium, *J. Geophys. Res.*, *67*, 1965–1974.

Norton, D., and B. Dutrow (2001), Complex behaviour of magma-hydrothermal processes: role of supercritical fluid, *Geochim. Cosmochim. Acta*, *65*(21), 4009–4017.

Ohba, T., H. Taniguchi, H. Oshima, M. Yoshida, and A. Goto (2002), Effect of explosion energy and depth on the nature of explosion cloud – a field experimental study., *J. Volcanol. Geotherm. Res.*, *115*, 33–42.

Ohba, T., H. Taniguchi, T. Miyamoto, S. Hayashi, and T. Hasenaka (2007), Mud plumbing system of an isolated phreatic eruption at Akita Yakeyama volcano, northern Honshu, Japan, *J. Volcanol. Geotherm. Res.*, *161*, 35–46.

Ohl, C.-D., T. Kurz, R. Geisler, O. Lindau, and W. Lauterborn (1999), Bubble dynamics, shock waves and sonoluminescence, *Phil. Trans. R. Soc. Lond. A*, *357*, 269–294.

Ozima, M., and M. Tatsumoto (1997), Radiation-induced diamond crystallization: origin of carbonados and its implications on meteorite nano-diamonds, *Geochim. Cosmochim. Acta*, *61*(2), 369–376.

Phipps Morgan, J., T. Reston, and C. Ranero (2004), Contemporaneous mass extinctions, continental flood basalts, and 'impact signals': are mantle plume-induced lithospheric

gas explosions the causal link ?, *Earth and Planetary Science Letters*, *217*, 263–284, doi:10.1016/S0012-821X(03)00602-2.

Planas-Cuchi, E., J. Salla, and J. Casal (2004), Calculating overpressure from BLEVE explosions, *Journal of Loss Prevention in the Process Industries*, *17*, 431–436, doi:10. 1016/j.jlp.2004.08.002.

Rayleigh, L. (1917), On the pressure developed in a liquid during the collapse of a spherical cavity, *Phil. Mag.*, *34*, 94–98.

Reid, R. (1983), Rapid phase transitions from liquid to vapor, *Advances in Chemical Engineering*, *12*, 105–208.

Richet, P., and A. Polian (1998), Water as a dense icelike component in silicate glasses, *Science*, *281*, 396–398.

Richet, P., A. Whittington, F. Holtz, H. Behrens, S. Ohlhorst, and M. Wilke (2000), Water and the density of silicate glasses, *Contrib. Mineral. Petrol.*, *138*, 337–347.

Salla, J., M. Demichela, and J. Casal (2006), BLEVE: a new approach to the superheat limit temperature, *Journal of Loss Prevention in the Process Industries*, *19*, 690–700, doi:10.1016/j.jlp.2006.04.004.

Shmulovich, K., L. Mercury, R. Thiéry, C. Ramboz, and M. El Mekki (2009), Experimental superheating of pure water and aqueous solutions, *Geochim. Cosmochim. Acta*, (accepted).

Sparks, R. (1978), The dynamics of bubble formation and growth in magmas: a review and analysis, *J. Volcanol. Geotherm. Res.*, *3*, 1–37.

Spieler, O., B. Kennedy, U. Kueppers, D. Dingwell, B. Scheu, and J. Taddeuci (2004), The fragmentation threshold of pyroclastic rocks, *Earth and Planetary Science Letters*,

226, 139–148, doi:10.1016/j.epsl.2004.07.016.

Suslick, K., Y. Didenko, M. Fang, T. Hyeon, K. Kolbeck, W. McNamara, M. Mdleleni, and M. Wong (1999), Acoustic cavitation and its chemical consequences, *Phil. Trans. R. Soc. Lond. A*, *357*, 335–353.

Taniguchi, H., and K. Suzuki-Kamata (1993), Direct measurement of overpressure of a volcanic blast on the June 1991 eruption at Unzen volcano, Japan, *Geophys. Res. Lett.*, *20*(2), 89–92.

Theofanous, T. (1995), The study of steam explosions in nuclear systems, *Nuclear Engineering and Design*, *155*, 1–26.

Thiéry, R. (1996), A new object-oriented library for calculating high-order multivariable derivatives and thermodynamic properties of fluids with equations of state, *Computers & Geosciences*, *22*(7), 801–815.

Thomas, N., C. Jaupart, and S. Vergniolle (1994), On the vesicularity of pumice, *J. Geophys. Res.*, *99*, 15,633–15,644.

Van den Berg, A., and A. Lannoy (1993), Methods for vapour cloud explosion blast modeling, *Journal of Hazardous Materials*, pp. 151–171.

Venart, J., G. Rutledge, K. Sumathipala, and K. Sollows (2004), To BLEVE or not to BLEVE: anatomy of a boiling liquid expanding vapor explosion, *Process Safety Progress*, *12(2)*, 67–70.

Voight, B. (1981), Time scale for the first moments of the May 18 eruption, in *The 1980 Eruptions of Mount St. Helens*, *U.S. Geol. Surv. Prof. Paper*, vol. 1250, edited by P. Lipman and D. Mullineaux, pp. 69–86, Washington, U.S.

Wagner, W., and A. Pruss (2002), The IAPWS formulation 1995 for the thermodynamic properties of ordinary water substance for general and scientific use, *J. Phys. Chem. Ref. Data*, *31*, 387–535.

Wohletz, K. (1983), Mechanisms of hydrovolcanic pyroclast formation: Grain-size, scanning electron microscopy, and experimental studies, *J. Volcanol. Geotherm. Res.*, *17*(1–4), 31–63.

Wohletz, K. (1986), Explosive magma-water interactions: thermodynamics, explosion mechanisms, and field studies, *Bull. Volcanol.*, *48*, 245–264.

Wohletz, K. (2002), Water/magma interaction: some theory and experiments on peperite formation, *J. Volcanol. Geotherm. Res.*, *114*, 19–35.

Wohletz, K., and H. Heiken (1992), *Volcanology and Geothermal Energy*, 432 pp., Univer. California Press.

Wohletz, K., T. McGetchin, M. S. II, and E. Jones (1984), Hydrodynamic aspects of caldera-forming eruptions: numerical models, *J. Geophys. Res.*, *89*(B10), 8269–8285.

Xiao, C., and D. Heyes (2002), Cavitation in stretched liquids, *Proc. R. Soc. Lond. A*, *458*, 889–910.

Yu, C., and J. Venart (1996), The boiling liquid collapsed bubble explosion (BLCBE): a preliminary model, *Journal of Hazardous Materials*, *46*, 197–213.

Zhang, Y. (1999), A criterion for the fragmentation of bubbly magma based on the brittle failure theory, *Nature*, *402*, 648–650.

Zhang, Y. (2000), Energetics of gas-driven limnic and volcanic eruptions, *J. Volcanol. Geotherm. Res.*, *97*, 215–231.

Zhang, Y., B. Sturtevant, and E. Stolper (1997), Dynamics of gas-driven eruptions: exper-

imental simulations using CO_2-H_2O-polymer system, *J. Geophys. Res.*, *102*, 3077–3096.

Zheng, Q. (1991), Liquids under tension and glasses under stress, Ph.D. thesis, Purdue

University, West Lafayette, Ind.

Zheng, Q., D. Durben, G. Wolf, and C. Angell (1991), Liquids at large negative pressures:

water at the homogeneous nucleation limit, *Science*, *254*, 829.

Zimanowski, B., V. Lorenz, and G. Fröhlich (1986), Experiments on phreatomagmatic

explosions with silicate and carbonatitic melts, *J. Volcanol. Geotherm. Res.*, *30*, 149–

155.

Zimanowski, B., G. Fröhlich, and V. Lorenz (1991), Quantitative experiments on

phreatomagmatic explosions, *J. Volcanol. Geotherm. Res.*, *48*(3–4), 341–358.

Zimanowski, B., G. Fröhlich, and V. Lorenz (1995), Experiments on steam explosion by

interaction of water with silicate melts, *Nuclear Engineering and Design,*, *155*, 335–343.

Zimanowski, B., R. Büttner, and V. Lorenz (1997a), Premixing of magma and water in

MFCI experiments, *Bull. Volcanol.*, *58*, 491–495.

Zimanowski, B., R. Büttner, V. Lorenz, and H.-G. Häfele (1997b), Fragmentation of

basaltic melt in the course of explosive volcanism, *J. Geophys. Res.*, *102*, 803–814.

Figure 1. Water volume fraction (f_v) in a mixture of melt, crystals and water as a function of the pressure P and temperature T, and for a water mass fraction of 5 % (A) and 15 % (B). A value of 2500 kg/m^3 has been chosen for the density of the melt and solids. The density of water is calculated with the equation of state of *Wagner and Pruss* [2002]). Lines are iso-f_v curves. In figure A, the corresponding density of the aqueous phase is indicated between parentheses in kg/m^3.

Figure 2. The stable, metastable and unstable fields of water projected in the $T-v$ space. The full lines separating the stable and metastable regions are the binodal curves: the first branch, noted L(G), refers to the saturated liquid water; whereas the other one, noted G(L), refers to the saturated steam. Both branchs join to the critical point (noted CP). The dashed curves are the two spinodal curves, which start from the critical point and delimit the unstable field from the metastable region. The first one, noted Sp(L), is the liquid spinodal curve; and the second one, noted Sp(G), is the gas spinodal curve.

Figure 3. $P-T$ diagram illustrating the different processes generating fluid instability. Solid line: the saturation curve (Sat.). Dotted lines: the liquid spinodal curve (Sp(L)) and the gas spinodal curve (Sp(G)). These three curves meet at the critical point (CP).

Figure 4. $T - U$ diagram used for estimating the mechanical work produced by isentropic expansions. This diagram includes several types of curves: (1) isobars (full thin lines), calculated at 1, 10, 50, 100, 200, 300 500 and 1000 bar; (2) isentropic decompression curves (dashed lines) for a monophasic system; and (3) isentropic decompression curves (dashed lines) for a biphasic system. Isentropic curves are labeled by their temperature at 1000 bar. Other elements of the diagram are the binodals (thick solid lines) L(G) and G(L); and the spinodals (dotted curves) Sp(L) and Sp(G).

Figure 5. $T - H$ diagram used for estimating isobaric heat transfer and mechanical work produced by isenthalpic or isentropic fluid circulations. This diagram includes several types of curves: (1) isobars (full thin lines), calculated at 1, 10, 50, 100, 200, 300, 500 and 1000 bar; (2) isentropic decompression curves (dashed lines) for a monophasic system; and (3) isentropic decompression curves (dashed lines) for a biphasic system. Isentropic curves are labeled by their temperature at 1000 bar. Other elements of the diagram are the binodals (thick solid lines) L(G) and G(L); and the spinodals (dotted curves) Sp(L) and Sp(G).

Figure 6. $P - T$ diagram showing the mechanical energy released by the reversible isentropic expansion of hot steam (in J/g of water) as a function of the initial pressure P and temperature T in the magmatic chamber. Thick solid lines: total work ($W_U = U_3 - U_5$) produced in the monophasic and biphasic fields. Thick dashed lines: mechanical work ($W_U = U_3 - U_4$) produced in the monophasic region. Dotted lines: isotherms of the condensation temperature (in K) of the steam at 1 bar. Below the isotherm 373 K, both curves of monophasic and total works are coincident.

Figure 7. The expansion work (J/g of water) of a liquid-gas mixture against atmospheric pressure as a function of the initial saturation temperature. The full line indicates energies calculated for an isentropic decompression process, whereas the dashed curve is calculated for an irreversible adiabatic expansion. L(G), G(L) and CP represent respectively expansion works calculated for a saturated liquid, a saturated steam and a critical fluid.

Figure 8. $P - T$ diagram showing the mechanical work (full solid lines, in J/g of water) released by the irreversible adiabatic expansion of hot and pressurized steam as a function of the initial $P - T$ conditions. Dashed lines indicate the liquid fraction (in mass percentage) of the gas-liquid mixture at a final state of 1 bar and 100°C. The field to the right of the 0% curve indicates the generation of superheated steams at 1 bar (i.e. with a final temperature above 100°C).

Figure 9. The mass liquid fraction of the liquid-gas mixture at 100°C and 1 bar produced by the depressurization of a saturated liquid (full curve) or saturated steam (dashed curve), as calculated by three types of decompression processes, i.e. isentropic, isenthalpic and irreversible expansions.

Figure 10. The mechanical work (in J/g of water) produced by liquid vaporization, as a function of the boiling temperature.

Figure 11. $T - W$ diagram to calculate the work ($W = H - U$, in J/g of water) produced by fluid isobaric expansion as a function of the initial and final temperatures. For example, to calculate the expansion work done by heating the fluid from point A ($T_A = 694$ K) to point point B ($T_B = 975$ K) at constant pressure (here 1 bar), one makes the difference $W_B - W_A$ ($= 450 - 320 = 130$ J/g). Dotted lines are projections of the spinodal curves Sp(L) and Sp(G). Full thick lines are projections of the binodal curves L(G) and G(L). Thin solid lines are the isobars calculated at pressures of 1, 10, 50, 100, 200, 300, 500 and 1000 bar.

Figure 12. $P-T$ diagram showing the work produced by the isobaric and isothermal exsolution of water from magma (in J/g of exsolved water) at fixed pressure P and temperature T.

Figure 13. $P - H$ diagram. Thick solid curves: binodal L(G) and G(L) curves. Thick dotted curves: spinodal Sp(L) and Sp(G) curves. Thin dashed curves: isotherms calculated at $T = 200$, 300, 350, 374 (critical isotherm), 390, 500, 750, 1000 and 1227°C. Thin solid lines: isentropic expansion curves labeled by the initial fluid temperatures at 1000 bar. Majuscule letters refer respectively to: A: Liquid-dominated geothermal systems of low enthalpy. B: High-pressure hydrothermal systems of medium enthalpy. C: Vapour-dominated geothermal systems of high enthalpy. D: Exsolved magmatic, hot and pressurized, steams of vulcanian and plinian volcanic systems. E: Hot and low-pressure steams produced by superficial phreato-magmatism.

Table 1. List of symbols.

Symbol	Description
T	temperature
P	pressure
v	molar volume, m^3/mol
A	Helmholtz free energy
H	enthalpy
U	internal energy
S	entropy
W	mechanical work
ρ	density (kg/m^3)
$M_{\mathrm{H_2O}}$	molar weight of water, 0.018 kg/mol
f	mass (or molar) liquid fraction in a biphasic liquid-gas mixture
f_v	volume liquid fraction in a biphasic liquid-gas mixture
T_i, P_i	initial temperature and pressure
T_f, P_f	final temperature and pressure
T_c	water critical temperature, 374°C, 647.096 K
T_{sat}	saturation temperature, 100°C, 373.15 K at 1 bar
T_{sp}	liquid spinodal temperature at 1 bar, 320.45°C , 593.6 K
T_{hn}	spontaneous homogeneous nucleation temperature, 304°C, 577 K at 1 bar
T_L	Leidenfrost temperature
c_v, c_P	isochoric and isobaric heat capacity, J/kg/K
ζ	conversion factor of the mechanical energy into kinetic and potential energy $(0 \leq \zeta \leq 1)$
$c_{U,S}$, $c_{H,S}$	isentropic heat capacities, J/kg/K
m_r	pyroclasts mass driven by one kg of water
V	flow velocity of ejected water and pyroclasts, m/s
$\overline{v}_{\mathrm{H_2O}}$	partial molar volume of H$_2$O in silicate melts

Table 2. Comparative summary of the two fundamental kinetics, nucleation-growth and spin-odal decomposition, of first-order phase transitions for an initial fluid. Note that the explosivity property is relevant only for the boiling of a liquid.

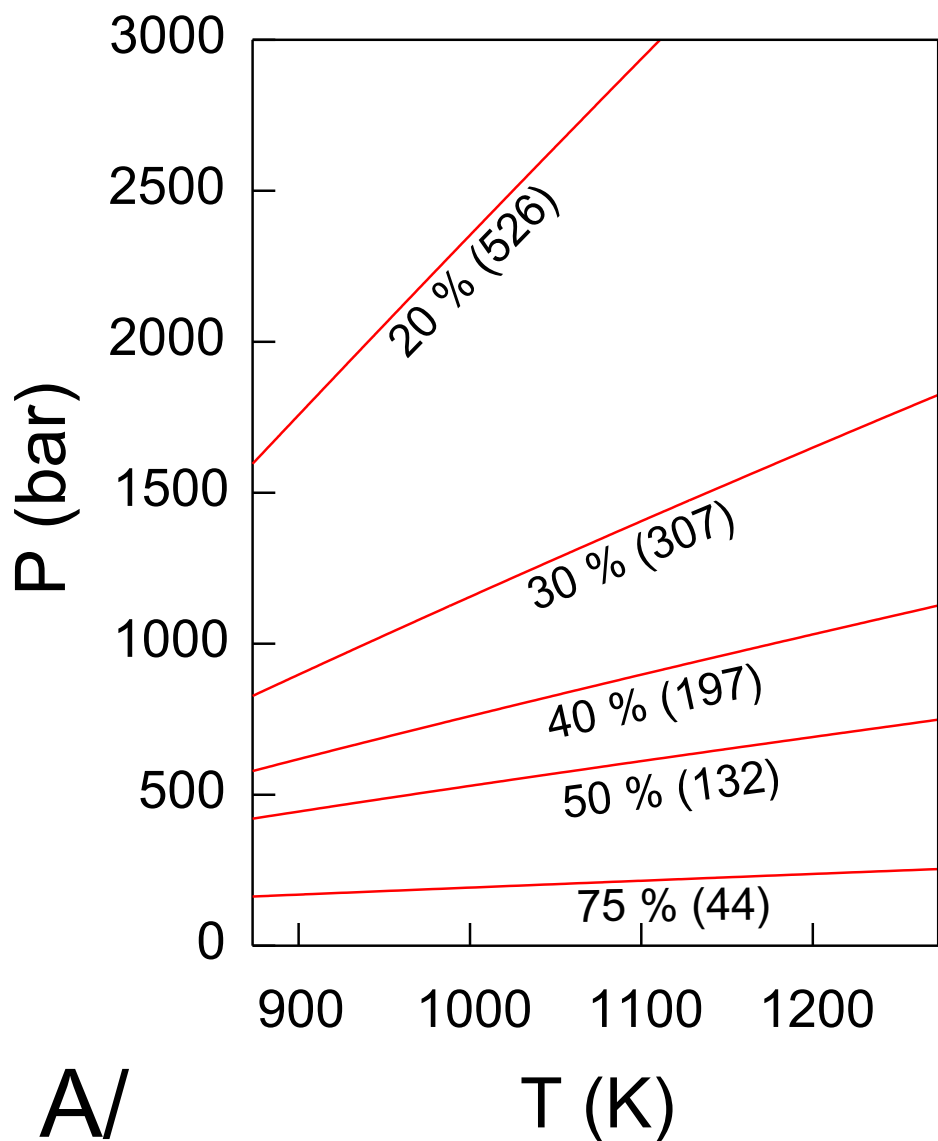| Main Characteristics		Nucleation-Growth	Spinodal Decomposition
Starting state		Metastable	Unstable
Process nature		Activated	Spontaneous
Initial density fluctuations			
	Localisation	At nucleation sites	Everywhere
	Amplitude	High	Low
	Wavelength	Short	Long
Final spatial biphasic pattern		Well separated liquid and gas	Imbricated biphasic association
Reactive zone		Boiling front	Everywhere
Mean diffusion length of heat and/or mass transfer		Large	Small
Transformation rate		Low to high	Very high
Explosivity		Low to high	Very high

Table 3. Calculation example of the mechanical energy released by a fluid isentropic decompression (*: calculated on the gas branch of the saturation curve), either in the case of a transient process, or a flow process.

State	Transient Process	Flow Process
Point 3 (900 K, 1000 bar)	$U_3 = 2711$ J/g	$H_3 = 3003$ J/g
Point 4* (615 K, 149 bar)	$U_4 = 2465$ J/g	$H_4 = 2615$ J/g
Point 5 (373.15 K, 1 bar)	$U_5 = 1799$ J/g	$H_5 = 1911$ J/g
% of liquid at point 5	34 %	34 %
Mechanical energy	$W_U = 912$ J/g	$W_H = 1092$ J/g

Table 4.   Classification of the different hydrothermal and volcanic system types as a function of their nature, environment, energy source, energy amplitude, and explosivity. [1]: these values are calculated by assuming an equal contribution of (1) magma exsolution and decompression, and (2) liquid boiling and steam heating.
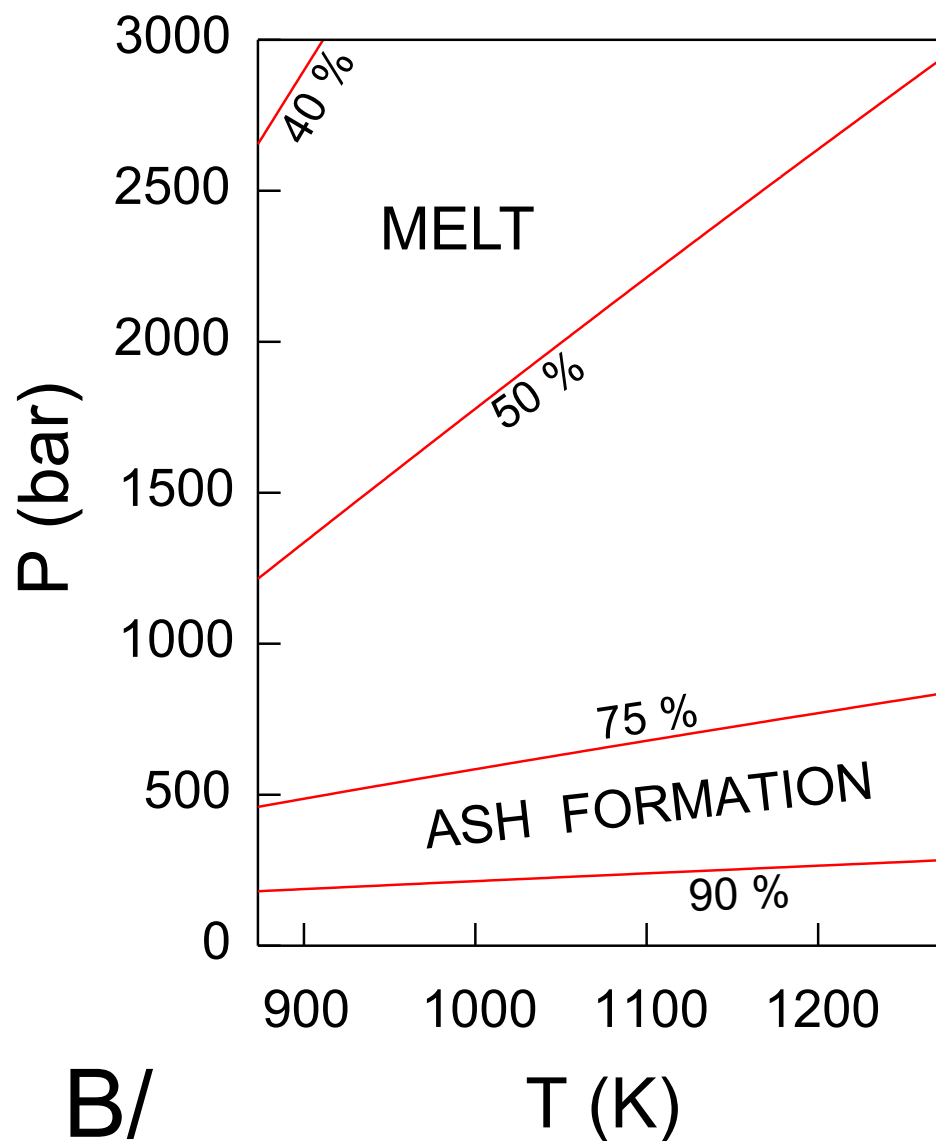
Type	Fluid nature	Environment	Energy source	Energy ($J/g\ H_2O$)	Explosivity
A	Liquid	Liquid-dominated geothermal systems	Decompression	0–100	Weak
B	Super-critical	Deep hydrothermal systems	Decompression	150–200	Low to high
C	Steam	Vapour-dominated geothermal systems	Decompression	100–150	Weak
D	Steam	Vulcanian and Plinian volcanism	Exsolution and decompression TOTAL	450–600 200–400 650–1000	High
E	Liquid	Surtseyan volcanism, superficial phreato-magmatism	Boiling and decompression TOTAL[1]	200–600 100–300 150–450	High
E+D	Liquid and steam	Phreato-plinian volcanism	Exsolution, decompression and boiling TOTAL[1]	450–600 200–400 200–600 425–800	Very high

5 wt % H_2O

A/

P (bar) vs T (K)

20 % (526)
30 % (307)
40 % (197)
50 % (132)
75 % (44)

15 wt % H_2O

B/

P (bar) vs T (K)

40 %
MELT
50 %
75 %
ASH FORMATION
90 %